

Received April 4, 2021, accepted April 13, 2021, date of publication April 16, 2021, date of current version April 26, 2021.

Digital Object Identifier 10.1109/ACCESS.2021.3073693

Sloping-Invariance for Nonferrous Metallic Slabs at Multiple Frequencies by Eddy Current Sensors

YUE DU¹, ZHIJIE ZHANG¹, (Member, IEEE), WULIANG YIN^{1,2}, (Senior Member, IEEE), AND GRZEGORZ TYTKO³

¹School of Instrument and Electronics, North University of China, Taiyuan 030051, China

²Department of Electrical and Electronic Engineering, The University of Manchester, Manchester M13 9PL, U.K.

³The Institute of Electronics, Silesian University of Technology, 44-100 Gliwice, Poland

Corresponding authors: Zhijie Zhang (zhangzhijie@nuc.edu.cn) and Wuliang Yin (wuliang.yin@manchester.ac.uk)

This work was supported in part by the Shanxi International Science and Technology Cooperation Project under Grant 201803D421038, and in part by the Shanxi 1331 Project Key Subject Construction.

ABSTRACT Eddy current sensors have been widely applied to various measurements, whereas it is still obscure if these measurement techniques are workable for sloping samples. We start from a modified Dodd and Deeds's analytical solution for finite-size samples and find that the pseudo-linearity exists in the magnitude-phase curve of the theoretical mutual inductance. The curves for different conductivities have no intersections. The experiments for verifying the pseudo-linearity are conducted at multiple frequencies from 20 kHz to 100 kHz. We subsequently involve the sloping samples in our simulations and experiments at 20 kHz. The pseudo-linearity preserves in both the simulated and experimental results. To characterize this pseudo-linearity, we resort to the method of least squares. The obtained intercepts for the same conductivity at different tilting angles are almost the same. Hence the intercept is independent of the tilting angle. The intercepts for different conductivities are clearly separated. Thus, the intercepts for non-sloping samples can be directly utilized as the criterion to classify sloping samples. We then test the classification process at multiple frequencies, which works properly at all the frequencies. Our classification rates are advanced compared to those in the literature. This sloping-invariance (that is the tilting-angle-independent intercept) might make the eddy current sensors find wider applications.

INDEX TERMS Eddy current sensor, conductivity classification, sloping-invariance, tilting angle, nonferrous metallic slab.

I. INTRODUCTION

The eddy current sensors have been widely used in the material property measurement [1], [2], displacement measurement [3], [4], crack detection [5], [6] and geometric measurement [7]–[9]. Most of the researches about eddy current sensors only consider the non-sloping samples, which implies that the sample is parallel to the coils. The ramps, however, might appear when using the industrial metal-cutting machine to cut the metallic scraps and then recycle them. It is important to explore such a case to improve the measurement robustness. One exasperated factor that makes an adverse effect on the application of conductivity classification is the liftoff due to the ramps that make the distance between the samples and the coils inconstant. There have been considerably efforts paid to reduce the

unfavorable effect from the liftoff. It was reported in [10] that the phase signature extracted from the spectral response of the pulsed eddy current sensors for thickness measurements is immune to liftoff effect. Other techniques contain utilizing the equivalent transformer secondary impedance [11], the compensated peak frequency [12] and the liftoff point of intersection [13]. Based on the conclusion about the liftoff-independent phase [14] (which accurately changes slowly with the liftoff for the finite-size sample), we are dedicated to finding the quantity that is immune to the tilting angle of the sloping metallic slabs in this paper.

There are some reported works recently [15], [16] that manage to classify sloping metallic samples. Two different classification schemes are presented, which are moving the sample (resulting in multi-valued mutual inductance curves) and moving the sensors (resulting in single-valued mutual inductance curves). The former one needs to be combined with photoelectric sensors to achieve the classification.

The associate editor coordinating the review of this manuscript and approving it for publication was Xiaokang Yin¹.

The latter one only uses the eddy current sensor. The sloping metallic samples have been successfully classified in these works. The formulations of the corresponding classification algorithms need the measurements of the mutual inductance for the sloping conductive samples. Nonetheless, the sloping-invariance found in this work from non-sloping samples can be directly utilized as the criterion to classify sloping samples. Moreover, the classifiable tilting angle is restricted within 9.0° in [15], and the operating frequency in [16] is 40 kHz, which is one of the frequencies used in this work.

In this paper, we manage to find a quantity that is independent of the tilting angle of the sloping metallic slab. We first give the analytical solution of the mutual inductance for the model of two coils above a finite-size metallic slab in Section II. It is found that the mutual inductance curve is pseudo-linear in the form of phase and normalized magnitude at the liftoff from 1 mm to 5 mm. We then conduct experiments in Section III to verify this pseudo-linearity with non-sloping samples at multiple frequencies. Because of the existence of this pseudo-linearity, we utilize the method of least squares to obtain the slopes and intercepts. Due to the lack of analytical models of two coils above the sloping metallic plate, we choose to conduct simulations and experiments to explore the effects that might be made by sloping the sample in Section IV. It is shown that the simulated results and experimental results are in great agreement with each other. The experimental results indicate that the pseudo-linearity and intercepts are not affected by sloping the samples. Based on the sloping-invariance, a complete process to classify the sloping metallic slabs is developed. In Section V, we test the classification process under a broad frequency spectrum.

II. THEORETICAL FOUNDATION

The analytical solution of the model of a coil above a two-conductor plane was first given by Dodd and Deeds [17]. Based on this analytical solution of the vector potential, the double-coil case is analytically solved [14]. The derived mutual inductance difference between the object field and empty field is given by [18]

$$\Delta L(\omega) = K \int_0^\infty \frac{P^2(\alpha)}{\alpha^6} A(\alpha)\phi(\alpha) d\alpha \quad (1)$$

where

$$\phi(\alpha) = \frac{(\alpha_1 + \mu\alpha)(\alpha_1 - \mu\alpha) - (\alpha_1 + \mu\alpha)(\alpha_1 - \mu\alpha)e^{2\alpha_1 c}}{-(\alpha_1 - \mu\alpha)(\alpha_1 - \mu\alpha) + (\alpha_1 + \mu\alpha)(\alpha_1 + \mu\alpha)e^{2\alpha_1 c}} \quad (2)$$

$$\alpha_1 = \sqrt{\alpha^2 + j\omega\sigma\mu_0} \quad (3)$$

$$K = \frac{\pi\mu_0 N^2}{(l_1 - l_2)^2 (r_1 - r_2)^2} \quad (4)$$

$$P(\alpha) = \int_{\alpha r_1}^{\alpha r_2} x J_1(x) dx \quad (5)$$

$$A(\alpha) = (e^{-\alpha l_1} - e^{-\alpha l_2})^2 \quad (6)$$

where α is the spatial frequency, ω is the excitation angular frequency, σ is the electrical conductivity, μ_0 is the vacuum permeability, c is the thickness of the sample, N is the number of turns of the coil, $l_2 - l_1$ is the height of the eddy current sensor, r_1 is the radius of ferrite, r_2 is the radius of the eddy current sensor, and J_1 is the Bessel function of the first kind. It was found in [19] that the integration range in (1) can be reduced to the range from $3.518/r_s$ to ∞ when the sample is finitely large because the variable α is inversely proportional to r_s , the radius of the sample, as shown in Fig. 1(a). Thus, the formula (1), when a finite-size sample is considered, is changed into

$$\Delta L(\omega) = K \int_{3.518/r_s}^\infty \frac{P^2(\alpha)}{\alpha^6} A(\alpha)\phi(\alpha) d\alpha \quad (7)$$

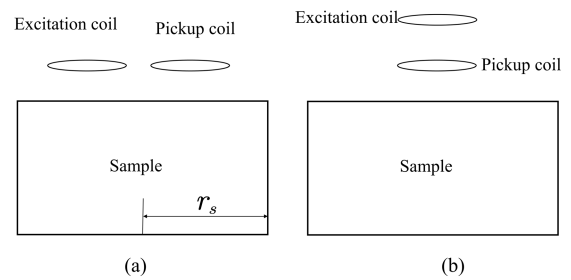


FIGURE 1. Diagrams of two types of eddy current sensors in which (a) is used in this work and (b) is used in [19].

where $3.518/r_s$ is obtained by solving the equation [19]

$$(\alpha r)^2 - 1 + \frac{\alpha r}{4J_1(\alpha r)}(2(J_0(\alpha r) - J_2(\alpha r)) - \alpha r(-3J_1(\alpha r) + J_3(\alpha r))) = 0 \quad (8)$$

where J_0 , J_1 , J_2 , and J_3 are the zero-, first-, second-, and third-order Bessel functions of the first kind.

Because of the difference between the eddy current sensor used in this work (see Fig. 1(a)) and that used in [19] (see Fig. 1(b)), it is necessary to analyze if (7) is still able to produce the well-known spectra [18], [20] of the real part and imaginary part of the mutual inductance or impedance. The corresponding spectra is depicted in Fig. 2 where the peak frequency shown in Fig. 2(a) is decreasing when the conductivity is increasing (see Table 1) and the real part in Fig. 2(b) decreases with the frequency, both of which are in accord with the corresponding results in [20]. The simulation information is given in Table 2. We then propose to analyze the mutual inductance in the form of phase and normalized magnitude when the liftoff is changing. This form is expressed by

$$|L|e^{j\psi} = \frac{|\Delta L|}{\max(|\Delta L|)} e^{j\psi} \quad (9)$$

where $|L|$ is the normalized magnitude, $\max(|\Delta L|)$ denotes the maximum of $|\Delta L|$, and

$$|\Delta L|e^{j\psi} = \Delta L_R + j\Delta L_I \quad (10)$$

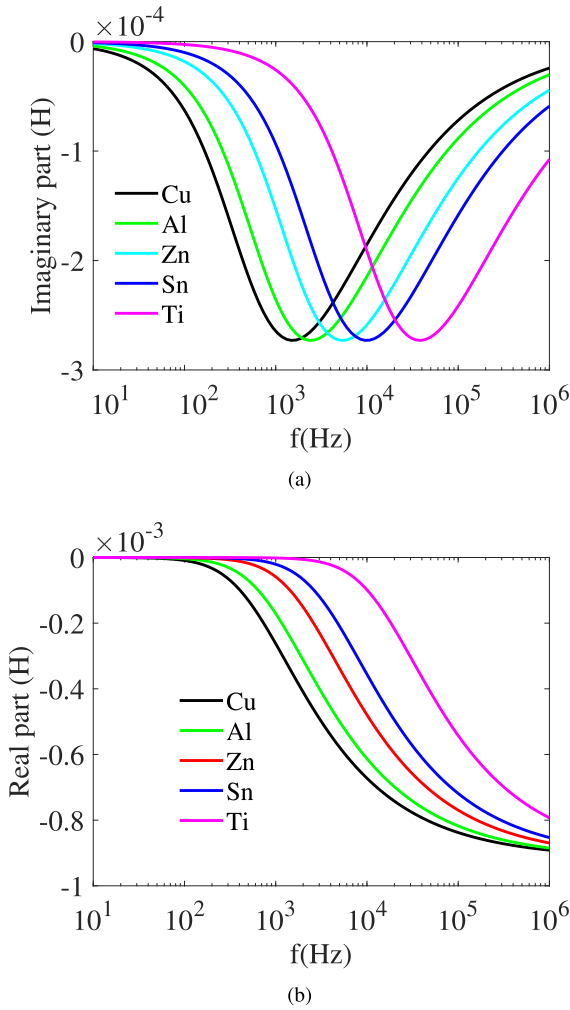


FIGURE 2. The spectra of the imaginary part (a) and the real part of the mutual inductance (b). (Note: Cu denotes copper; Al denotes aluminum; Zn denotes zinc; Sn denotes tin; Ti denotes titanium).

where

$$|\Delta L| = \sqrt{\Delta L_R^2 + \Delta L_I^2} \quad (11)$$

$$\psi = \tan^{-1}\left(\frac{\Delta L_I}{\Delta L_R}\right) \quad (12)$$

where $|\Delta L|$ is the magnitude, ψ is the phase, ΔL_R is the real part, and ΔL_I is the imaginary part. The liftoff changes from 1 mm to 5 mm. It has been demonstrated [14] that the phase is independent of the liftoff in the scenario of the sample with an infinite-size. In this work, the size of the sample is around four times the diameter of the coil, which is large enough that the phase in Fig. 3 has a slight change. This change, compared to the phase difference between different conductivities, can be taken as a pseudo-linear change. In the thickness measurement [21], [22], radius measurement [23] and conductivity/permeability [24]–[26] measurement, the sample usually has a horizontal surface. These measurement techniques would become applicable to more application scenarios if they are immune to sloping the sample. However, there is not any analytical solution for the sloping metallic plate so far,

TABLE 1. Electrical conductivity of metal.

Metal	Conductivity (S/m)
Copper	5.96×10^7
Aluminum	3.77×10^7
Zinc	1.69×10^7
Tin	0.92×10^7
Titanium	0.24×10^7

TABLE 2. Simulation information used to produce Fig. 2 and 3.

Parameters	Value
Radii of coils	1 mm
Spacing between two coils	3.5 mm
Height of coils	3 mm
Liftoff	1~5 mm
Thickness of the sample	1 cm
Size of the sample	1 cm
Excitation frequency	20 kHz

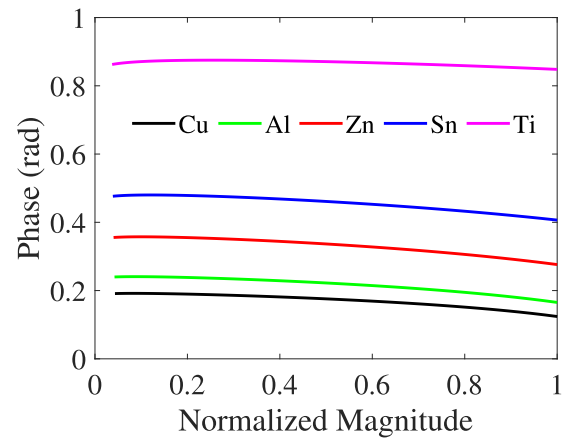


FIGURE 3. The mutual inductance in the form of phase and magnitude for five metallic samples. (Note: Cu denotes copper; Al denotes aluminum; Zn denotes zinc; Sn denotes tin; Ti denotes titanium).

to the best of our knowledge. Therefore, we involve sloping samples in the simulations and experiments to explore the effects introduced by the ramps.

III. EXPERIMENTAL SETUP

The main steps in the experiments include tilting the samples and moving the probe up and down. A schematic diagram of the setup including these steps is plotted in Fig. 4(a). The experimental setup (see Fig. 4(b)) consists of an excited coil, a pickup coil, a liftoff controller and an electromagnetic instrument [27], [28] for signal processing. This electromagnetic instrument operates from 5 kHz to 200 kHz in a step of 5 kHz, which can deliver data rate up to 256k/s (32k sample per channel). The metallic samples are $1 \times 1 \times 1 \text{ cm}^3$ cubes. The liftoff range in our experiments is [1 mm, 14 mm]. The sensor parameters [28] are listed in Table 3.

The experimental results of mutual inductance are depicted in Fig. 5, where the curve is rotating clockwise when the conductivity is increasing, the same as in [15], [16], [29]. By transforming the measured mutual inductance in the form

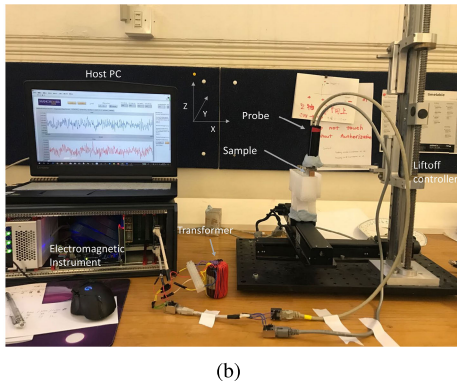
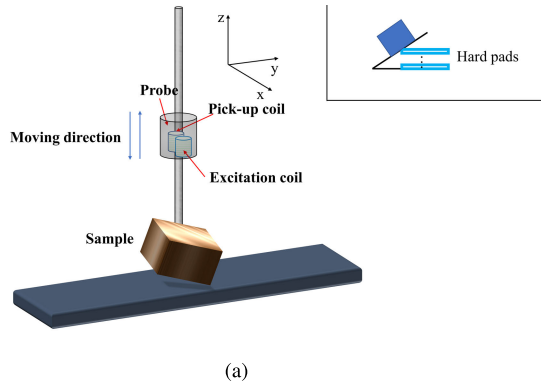


FIGURE 4. (a) The schematic diagram of the setup where the inset presents how to tilt the sample. (b) The experimental setup.

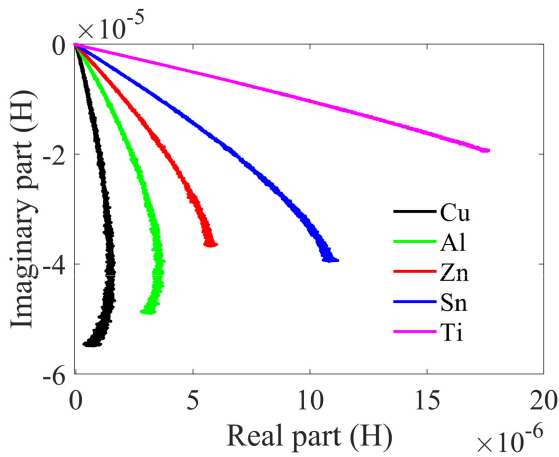


FIGURE 5. The measured mutual inductance in the form of real part and imaginary part for five non-sloping metallic samples at 20 kHz. (Note: Cu denotes copper; Al denotes aluminum; Zn denotes zinc; Sn denotes tin; Ti denotes titanium).

of phase and normalized magnitude, it is shown in Fig. 6 that there are certain pseudo-linear regions on the mutual inductance curves. The Fig. 6(a) is in great agreement with Fig. 3. In detail, the curves for different metallic samples are approximately parallel to each other.

Another observation is that the mutual inductance curves for all the samples in the range of (0.2, 0.8) behave to be hardly affected by the excitation frequencies in terms of the pseudo-linearity. This range corresponds to the liftoff

TABLE 3. Sensor parameters.

Parameters	Value
Inner Radii (Ex/Re)	0.75 mm/0.75 mm
Outer Radii (Ex/Re)	1.25 mm/1.5 mm
Spacing between two coils	3.5 mm
Height of coils	3 mm
Number of turns (Ex/Re)	160/200

Note: Ex denotes the excitation coil and Re denotes the pickup coil.

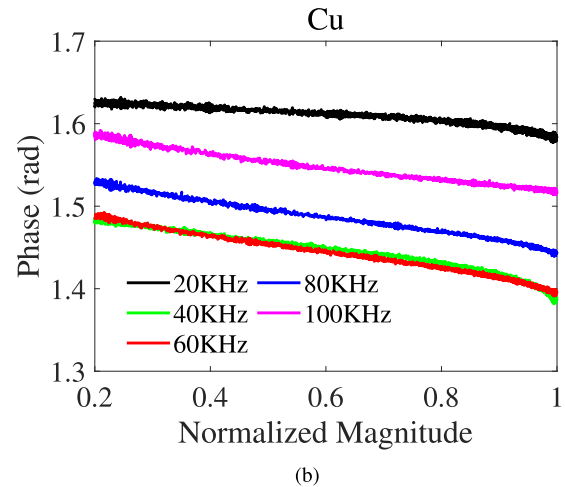
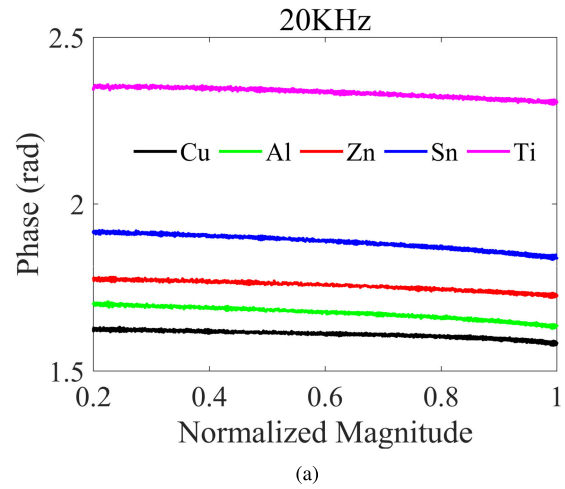


FIGURE 6. (a) Measured mutual inductance in the form of normalized magnitude and phase for five non-sloping metallic samples at 20kHz. (Note: Cu denotes copper; Al denotes aluminum; Zn denotes zinc; Sn denotes tin; Ti denotes titanium) (b) Measured mutual inductance for the sample copper at different excitation frequencies.

from 2 mm to 5 mm. Therefore, the pseudo-linear region of the liftoff for the metallic slabs is (2 mm, 5 mm). This pseudo-linearity implies that in this region, the phase changes with the magnitude at the same rate.

IV. SLOPING-INVARIANCE

In practical applications of eddy current sensors, such as sorting out metallic scraps, the scraps might be ramped. In this case, it is necessary to analyze the effects made by the ramps on the measurements. Thus, we conduct both the simulations

TABLE 4. Slopes and intercepts (with four significant figures) of the fitting linear functions of the mutual inductance curves for five metallic samples under six tilting angles at 20 kHz.

Metal	Cu		Al		Zn		Sn		Ti	
	Parameter (rad)		Slope	Intercept	Slope	Intercept	Slope	Intercept	Slope	Intercept
Angle										
0 °	-0.03465	1.633	-0.06470	1.715	-0.05189	1.788	-0.07868	1.936	-0.05502	2.369
2.9 °	-0.03649	1.634	-0.06792	1.709	-0.1038	1.791	-0.09589	1.933	-0.08862	2.362
5.7 °	-0.03965	1.619	-0.07662	1.713	-0.09152	1.785	-0.1052	1.925	-0.1080	2.364
8.5 °	-0.04062	1.621	-0.08645	1.719	-0.08268	1.780	-0.09787	1.927	-0.09144	2.354
11.3 °	-0.03956	1.622	-0.08145	1.720	-0.06163	1.775	-0.07450	1.926	-0.07759	2.371
14.0 °	-0.03926	1.628	-0.04626	1.720	-0.04913	1.776	-0.06612	1.930	-0.02825	2.356

and experiments for the sloping metallic samples to simulate the ramps. This approximation is available because the thickness of the samples is around ten times larger than the skin depth in our experiments. The simulations are implemented in ANSYS EM Suite 2020 R2. The simulation model is given in Fig. 7 where there are two coils and a sloping conductor. The simulation parameters of the coils and samples are the same as given in Table 2. The liftoff is the same as in the experiments, which ranges from 1 mm to 14 mm in a step of 0.2 mm. The simulated results are shown in Fig. 8, where the magnitude-phase curves for the same sample at different tilting angles are overlapping. Nonetheless, the curves for different samples are parallel to each other, which is exceedingly helpful for the conductivity classification. The reason for this phenomenon is that the phase differences introduced by different conductivities are much larger than those caused by tilting angles within 14.0°. In other words, the conductivity difference has more influence on the eddy current distribution than the tilting angle.

As is shown in Fig. 9, there are measured mutual inductance curves for five samples under six tilting angles. When the eddy current sensor is moved up and down, the minimum liftoff (which is the distance between the bottom of the coil and top of the sloping sample) is always kept to be 1mm and no change is made to the maximum liftoff. It can be concluded that although the samples are sloping, which indicates that the eddy current distribution becomes different from the non-sloping case, the phase still changes pseudo-linearly with the normalized magnitude, which is in great agreement with the simulated results. The phases of sloping samples are scattered around the curves belonging to the corresponding non-sloping ones. The parameters to represent the pseudo-linearity can be found by the method of least squares, given by,

$$\psi = k|L| + b \tag{13}$$

where

$$k = \frac{\sum_{n=1}^N |L_n| \psi_n - N \overline{|L|} \overline{\psi}}{\sum_{n=1}^N |L_n|^2 - N \overline{|L|}^2} \tag{14}$$

and

$$b = \overline{\psi} - k \overline{|L|} \tag{15}$$

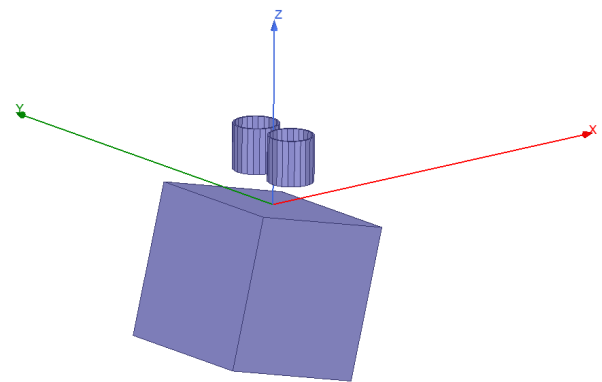


FIGURE 7. The simulation model consists of two coils and a sloping conductor, exported from ANSYS EM Suite 2020 R2.

where ψ is the phase, $|L|$ is the normalized magnitude, k is the slope, b is the intercept, N is the length of the measured data, $\overline{|L|}$ is the average of all the magnitudes, and $\overline{\psi}$ is the average of all the phases. The slopes and intercepts for five samples under six tilting angles at 20 kHz are listed in Table 4. Although the slopes are changing with the tilting angle for the same metal, the intercepts are pretty stable. As is shown in Fig. 10, the intercepts for the same metal have little variation. Therefore, it is easy to classify the sloping samples by the intercepts belonging to the non-sloping samples.

The process for extracting the tilting-angle-independent intercepts can be easily modified to a conductivity classification process that includes

- 1) Put the unknown sample under the probe that wraps up the eddy current sensor.
- 2) Move the probe up and down. The highest liftoff is 14mm and the lowest is 1mm. (The liftoff is the spacing between the bottom of the probe and the top of the sample)
- 3) Output the measured real parts and imaginary parts of the mutual inductance and transform them in the form of phase and magnitude.
- 4) Normalize the magnitude and choose the range to be (0.2 0.8).
- 5) Use the method of least squares to find the corresponding intercept.

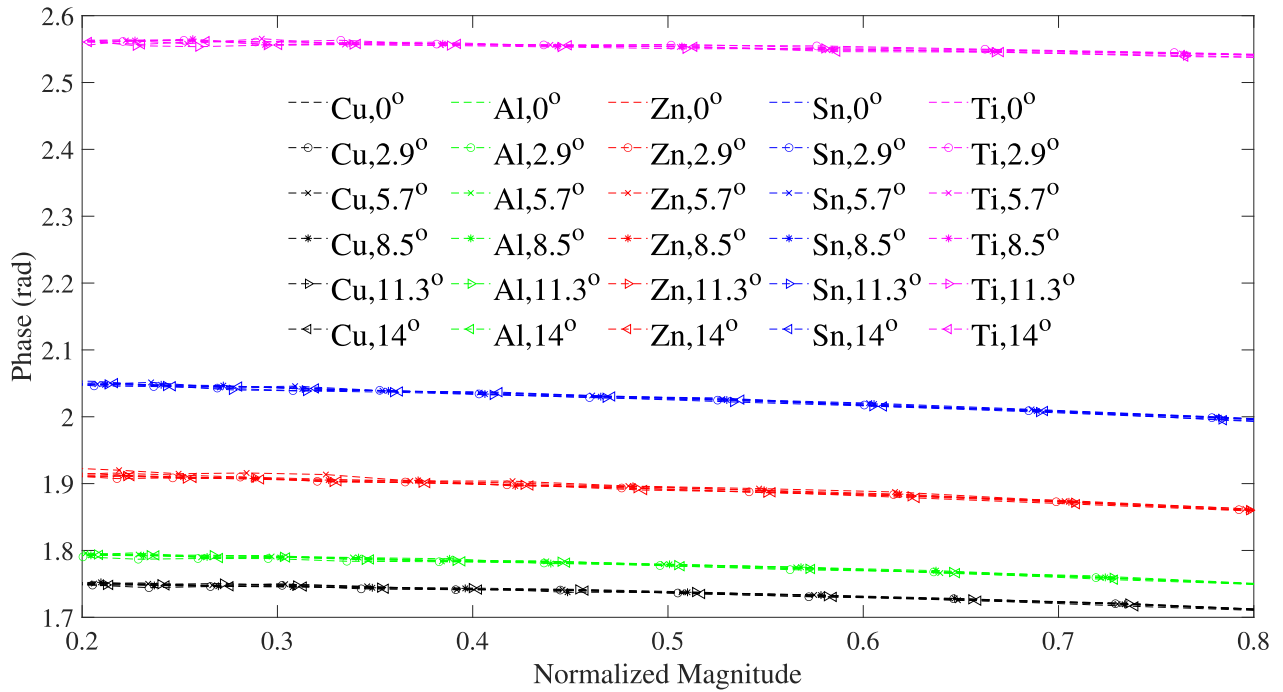


FIGURE 8. Simulated mutual inductance for five samples under six titling angles at 20 kHz, where the magnitude range is chosen to be (0.2, 0.8). (Note: Cu denotes copper; Al denotes aluminum; Zn denotes zinc; Sn denotes tin; Ti denotes titanium).

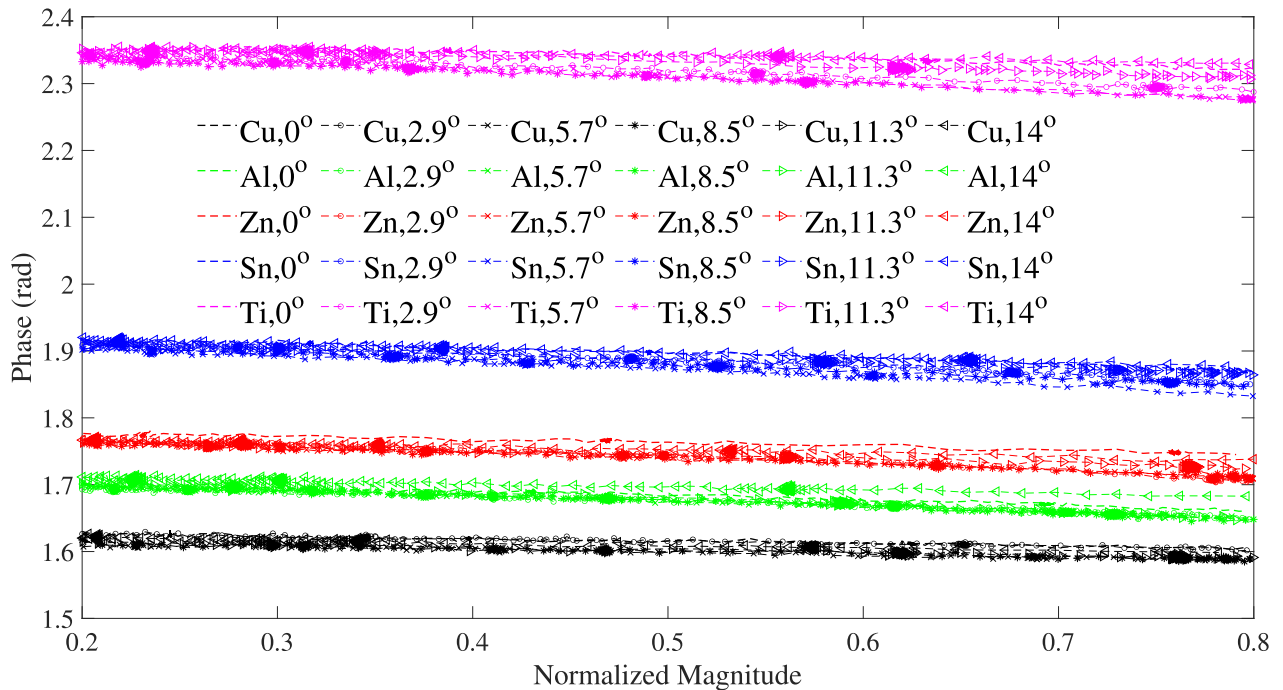


FIGURE 9. Measured mutual inductance for five samples under six titling angles at 20 kHz, where the magnitude range is chosen to be (0.2, 0.8). (Note: Cu denotes copper; Al denotes aluminum; Zn denotes zinc; Sn denotes tin; Ti denotes titanium).

- 6) Solve the differences between this intercept and five intercepts belonging to the five non-sloping metals.
- 7) Find the minimum absolute value of the differences and decide the conductivity of this unknown sample.

V. TESTS AT MULTIPLE FREQUENCIES

Since this pseudo-linearity is broadband for non-sloping samples as shown in Fig. 6(b), it is worth finding the spectral property of the tilting-angle-independent intercept by using the above process. Hence we conduct experiments at the

TABLE 5. Intercepts (with four significant figures) for five metallic samples under six tilting angles at 40 kHz and 60 kHz.

Intercept (rad) at Metal \ Angle	40 kHz					60 kHz				
	Cu	Al	Zn	Sn	Ti	Cu	Al	Zn	Sn	Ti
0 °	1.500	1.561	1.622	1.717	2.067	1.507	1.559	1.609	1.692	1.974
2.9 °	1.498	1.551	1.611	1.716	2.050	1.508	1.555	1.608	1.691	1.963
5.7 °	1.488	1.555	1.610	1.713	2.053	1.504	1.558	1.598	1.684	1.959
8.5 °	1.488	1.550	1.600	1.707	2.040	1.498	1.549	1.596	1.681	1.961
11.3 °	1.490	1.553	1.604	1.706	2.049	1.494	1.545	1.590	1.677	1.957
14.0 °	1.482	1.553	1.602	1.713	2.051	1.490	1.550	1.587	1.684	1.960

TABLE 6. Intercepts (with four significant figures) for five metallic samples under six tilting angles at 80 kHz and 100 kHz.

Intercept (rad) at Metal \ Angle	80 kHz					100 kHz				
	Cu	Al	Zn	Sn	Ti	Cu	Al	Zn	Sn	Ti
0 °	1.547	1.596	1.643	1.716	1.953	1.592	1.646	1.689	1.749	1.964
2.9 °	1.548	1.591	1.635	1.712	1.952	1.603	1.649	1.694	1.756	1.972
5.7 °	1.548	1.588	1.628	1.703	1.947	1.608	1.633	1.681	1.737	1.959
8.5 °	1.543	1.589	1.630	1.696	1.939	1.606	1.640	1.670	1.740	1.956
11.3 °	1.551	1.580	1.620	1.697	1.936	1.595	1.623	1.664	1.738	1.955
14.0 °	1.543	1.550	1.618	1.702	1.954	1.599	1.638	1.668	1.734	1.958

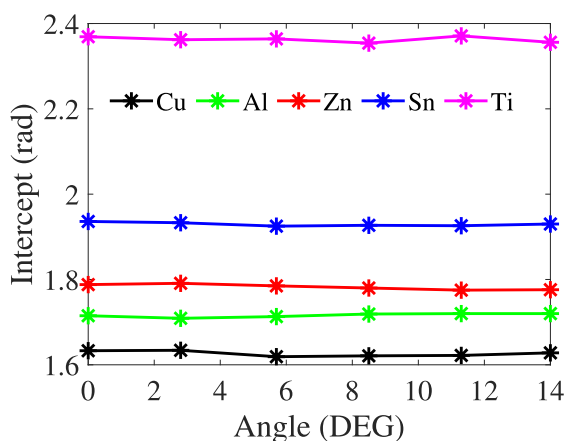


FIGURE 10. The distribution of the intercepts given in Table 4.

frequency from 40 kHz to 100 kHz for sloping samples. The results at 40 kHz and 60 kHz are shown in Table 5 where the slopes for the same conductivity are distributed closely, and the slopes for different conductivities are detached. The results at 80 kHz and 100 kHz are displayed in Table 6 where the slopes for the same conductivity still vary slightly except for the sample aluminum at 14.0 ° and 80 kHz. This intercept jumps from 1.580 to 1.550 that is extremely close to the intercepts belonging to the sample copper at 11.3 ° and 80 kHz. By conducting the seven-step classification process in Section IV, the intercepts for the non-sloping samples at frequencies from 40 kHz to 100 kHz constitute

the classification criterion, and the classification rates within 14.0° at these frequencies are 100%, 100%, 96%, and 100%, respectively. Our classification method by resorting to this sloping-invariance is more accurate compared to the classification rates in [15], [16], which are 95% within 9.0° and 96.7% within 14.0° at 40 kHz, respectively. Overall, the sloping-invariance is broadband and appropriate for the conductivity classification.

VI. CONCLUSION

The sloping-invariance (that is the tilting-angle-independent intercept) is found to support a conductivity classification process, within which only the measurements for non-sloping samples are needed as the criterion. We first find a certain liftoff region where the magnitude-phase curve can be taken as a pseudo-linear curve for the non-sloping samples. We then conduct experiments to verify this pseudo-linearity at multiple frequencies. The normalized magnitude range (0.2, 0.8) is chosen to exclude the drooping tails caused by increasing the frequency. We subsequently conduct simulations and experiments at 20 kHz for sloping samples. The pseudo-linearity preserves in both the simulated and experimental results. The method of least squares is then implemented to find the slopes and intercepts of the mutual inductance curves at 20kHz. It is observed that the intercepts for the same metallic sample with different tilting angles are distributed closely, and those for different samples are scattered distantly. This intercept-extraction process can be easily modified to classify the sloping metallic samples. Furthermore, it is shown in the

test results that the process is applicable to a broad frequency spectrum. Our classification rates are advanced than those in the literature. The sloping-invariance found in this work might help eddy current sensors find wider applications in the future.

REFERENCES

- [1] X. Chen and Y. Lei, "Electrical conductivity measurement of ferromagnetic metallic materials using pulsed eddy current method," *NDT E Int.*, vol. 75, pp. 33–38, Oct. 2015.
- [2] X. Ma, A. J. Peyton, and Y. Y. Zhao, "Eddy current measurements of electrical conductivity and magnetic permeability of porous metals," *NDT E Int.*, vol. 39, no. 7, pp. 562–568, Oct. 2006.
- [3] M. R. Nabavi and S. N. Nihtianov, "Design strategies for eddy-current displacement sensor systems: Review and recommendations," *IEEE Sensors J.*, vol. 12, no. 12, pp. 3346–3355, Dec. 2012.
- [4] M. R. Nabavi and S. Nihtianov, "A novel interface for eddy current displacement sensors," *IEEE Trans. Instrum. Meas.*, vol. 58, no. 5, pp. 1623–1632, May 2009.
- [5] L. Cheng and G. Y. Tian, "Surface crack detection for carbon fiber reinforced plastic (CFRP) materials using pulsed eddy current thermography," *IEEE Sensors J.*, vol. 11, no. 12, pp. 3261–3268, Dec. 2011.
- [6] G. Y. Tian, A. Sophian, D. Taylor, and J. Rudlin, "Multiple sensors on pulsed eddy-current detection for 3-D subsurface crack assessment," *IEEE Sensors J.*, vol. 5, no. 1, pp. 90–96, Feb. 2005.
- [7] W. Yin and A. J. Peyton, "Thickness measurement of non-magnetic plates using multi-frequency eddy current sensors," *NDT E Int.*, vol. 40, no. 1, pp. 43–48, Jan. 2007.
- [8] X. Mao and Y. Lei, "Thickness measurement of metal pipe using swept-frequency eddy current testing," *NDT E Int.*, vol. 78, pp. 10–19, Mar. 2016.
- [9] R. Xie, D. Chen, M. Pan, W. Tian, X. Wu, W. Zhou, and Y. Tang, "Fatigue crack length sizing using a novel flexible eddy current sensor array," *Sensors*, vol. 15, no. 12, pp. 32138–32151, Dec. 2015.
- [10] M. Fan, B. Cao, A. I. Sunny, W. Li, G. Tian, and B. Ye, "Pulsed eddy current thickness measurement using phase features immune to liftoff effect," *NDT E Int.*, vol. 86, pp. 123–131, Mar. 2017.
- [11] A. L. Ribeiro, H. G. Ramos, and J. C. Arez, "Liftoff insensitive thickness measurement of aluminum plates using harmonic eddy current excitation and a GMR sensor," *Measurement*, vol. 45, no. 9, pp. 2246–2253, Nov. 2012.
- [12] M. Lu, L. Yin, A. Peyton, and W. Yin, "A novel compensation algorithm for thickness measurement immune to lift-off variations using eddy current method," *IEEE Trans. Instrum. Meas.*, vol. 65, no. 12, pp. 2773–2779, Dec. 2016.
- [13] M. Fan, B. Cao, G. Tian, B. Ye, and W. Li, "Thickness measurement using liftoff point of intersection in pulsed eddy current responses for elimination of liftoff effect," *Sens. Actuators A, Phys.*, vol. 251, pp. 66–74, Nov. 2016.
- [14] W. Yin, R. Binns, S. J. Dickinson, C. Davis, and A. J. Peyton, "Analysis of the liftoff effect of phase spectra for eddy current sensors," *IEEE Trans. Instrum. Meas.*, vol. 56, no. 6, pp. 2775–2781, Dec. 2007.
- [15] Y. Du, Z. Zhang, W. Yin, S. Zhu, Z. Chen, and H. Xu, "Conductivity classification of non-magnetic tilting metals by eddy current sensors," *Sensors*, vol. 20, no. 9, p. 2608, May 2020.
- [16] Y. Du, Z. Zhang, W. Yin, S. Zhu, H. Xu, and Z. Chen, "A novel conductivity classification technique for non-magnetic tilting metals by eddy current sensors," *IEEE Access*, vol. 8, pp. 151125–151132, 2020.
- [17] C. V. Dodd and W. E. Deeds, "Analytical solutions to eddy-current probe-coil problems," *J. Appl. Phys.*, vol. 39, no. 6, pp. 2829–2838, May 1968.
- [18] W. Yin, A. J. Peyton, and S. J. Dickinson, "Simultaneous measurement of distance and thickness of a thin metal plate with an electromagnetic sensor using a simplified model," *IEEE Trans. Instrum. Meas.*, vol. 53, no. 4, pp. 1335–1338, Aug. 2004.
- [19] R. Huang, M. Lu, A. Peyton, and W. Yin, "Thickness measurement of metallic plates with finite planar dimension using eddy current method," *IEEE Trans. Instrum. Meas.*, vol. 69, no. 10, pp. 8424–8431, Oct. 2020.
- [20] M. D. O'Toole, N. Karimian, and A. J. Peyton, "Classification of non-ferrous metals using magnetic induction spectroscopy," *IEEE Trans. Ind. Informat.*, vol. 14, no. 8, pp. 3477–3485, Aug. 2018.
- [21] W. Yin, R. Huang, M. Lu, Z. Zhang, and A. Peyton, "Measurements of thickness for metallic plates with co-axial holes using a novel analytical method with the modified integration range," *IEEE Access*, vol. 8, pp. 198301–198306, 2020.
- [22] Y. Yu, D. Zhang, C. Lai, and G. Tian, "Quantitative approach for thickness and conductivity measurement of monolayer coating by dual-frequency eddy current technique," *IEEE Trans. Instrum. Meas.*, vol. 66, no. 7, pp. 1874–1882, Jul. 2017.
- [23] R. Huang, M. Lu, Z. Zhang, Q. Zhao, Y. Xie, Y. Tao, T. Meng, A. Peyton, T. Theodoulidis, and W. Yin, "Measurement of the radius of metallic plates based on a novel finite region eigenfunction expansion (FREE) method," *IEEE Sensors J.*, vol. 20, no. 24, pp. 15099–15106, Dec. 2020.
- [24] J. Xu, J. Wu, W. Xin, and Z. Ge, "Measuring ultrathin metallic coating properties using swept-frequency eddy-current technique," *IEEE Trans. Instrum. Meas.*, vol. 69, no. 8, pp. 5772–5781, Aug. 2020.
- [25] H. Wang, W. Li, and Z. Feng, "Noncontact thickness measurement of metal films using eddy-current sensors immune to distance variation," *IEEE Trans. Instrum. Meas.*, vol. 64, no. 9, pp. 2557–2564, Sep. 2015.
- [26] M. Lu, H. Xu, W. Zhu, L. Yin, Q. Zhao, A. Peyton, and W. Yin, "Conductivity lift-off invariance and measurement of permeability for ferrite metallic plates," *NDT E Int.*, vol. 95, pp. 36–44, Apr. 2018.
- [27] J. R. S. Avila, Z. Chen, H. Xu, and W. Yin, "A multi-frequency NDT system for imaging and detection of cracks," in *Proc. IEEE Int. Symp. Circuits Syst. (ISCAS)*, May 2018, pp. 1–4.
- [28] H. Xu, J. R. S. Avila, F. Wu, M. J. Roy, Y. Xie, F. Zhou, A. Peyton, and W. Yin, "Imaging X70 weld cross-section using electromagnetic testing," *NDT E Int.*, vol. 98, pp. 155–160, Sep. 2018.
- [29] C. Wang, M. Fan, B. Cao, B. Ye, and W. Li, "Novel noncontact eddy current measurement of electrical conductivity," *IEEE Sensors J.*, vol. 18, no. 22, pp. 9352–9359, Nov. 2018.



YUE DU received the B.S. degree from the School of Physics, Liaoning University, Shenyang, China. She is currently pursuing the M.S. degree with the School of Instrument and Electronics, North University of China, Shanxi, China. Her research interests include non-destructive testing, conductivity classification, and EMT imaging.



ZHIJIE ZHANG (Member, IEEE) received the B.Sc. degree in automation instrumentation from Tianjin University, Tianjin, China, in 1986, and the Ph.D. degree in mechatronic engineering from the Beijing Institute of Technology, Beijing, China, in 1998. He is currently a Professor with the School of Instrument and Electronics, North University of China, Taiyuan, Shanxi, China.



WULIANG YIN (Senior Member, IEEE) received the B.Sc. and M.Sc. degrees in electronic measurement and instrumentation from Tianjin University, Tianjin, China, in 1992 and 1995, respectively, and the Ph.D. degree in automotive electronics from Tsinghua University, Beijing, China, in 1999. He was appointed as a Mettler Toledo (MT) Sponsored Lecturer with the Department of Electrical and Electronic Engineering, School of Engineering, The University of Manchester, Manchester, U.K., in 2012, and was promoted to a Senior Lecturer, in 2016. He has authored one book and more than 230 articles, and was granted more than ten patents in the area of electromagnetic sensing and imaging. He was a recipient of the 2014 and 2015 Williams Award from the Institute of Materials, Minerals and Mining, and the Science and Technology Award from the Chinese Ministry of Education, in 2000.

GRZEGORZ TYTKO, photograph and biography not available at the time of publication.

• • •